Unbalanced Magnetic Pull in Fractional-Slot Brushless PM Motors

David G Dorrell, Mircea Popescu and Calum Cossar
Dept of Electronics and Electrical Engineering
University of Glasgow
Glasgow, G12 8LT, UK

Dan Ionel
Corporate Technology Centre
AO Smith Corp.
Milwaukee 53224, WI, USA

***Abstract*— This paper reports on an investigation into the unbalanced magnetic pull in brushless PM motors due to either magnetic asymmetry or rotor eccentricity. Several machines are investigated. These have different slot and pole number combinations. Some of the windings contain sub-harmonics and these are found to be more susceptible to UMP when there is rotor eccentricity and also to produce vibrating UMP. Consequent rotor poles are also found to produce high UMP under rotor eccentricity conditions.**

Keywords- Brushless permanent magnet motors, unbalanced magnetic pull, fractional slot

I. INTRODUCTION

Unbalanced magnetic pull (UMP) is usually associated with larger induction and synchronous machines under winding faults or rotor eccentricity conditions [1][2][3] and there is a large literature on this subject. However smaller machines are still subject to unbalanced magnetic pull [4][5] even without rotor anomalies. Unbalanced magnetic pull is important because it affects the wear on the bearings [6] as well as noise and vibration [7]. This is particularly the case in brushless servo motors were fractional slots are used [8]. This type of machine is studied here for the generalized case and several examples are used to highlight aspects of UMP generation in brushless PM machines. An analytical model is developed using rotating field theory and this is used to identify possible sources of UMP and the associated vibration frequencies. The example machines are analyzed use finite element analysis to obtain the magnitudes of the UMP and small rotor eccentricity is explored.

In this paper example machines are put forward. These consist of an 8 pole and 6 pole 9 slot machine as examples of a machines that can have UMP even when the rotor is centered. Results are obtained from the FEA to verify the method. The analysis is then extended to include rotor eccentricity and a 12 pole 18 slot and a 16 pole 18 slot machines are studied. These machines can have different winding layouts for single or double layer windings. 10 % static rotor eccentricity is put into these machines to assess the UMP under conditions that would produce UMP but not negate operation. If the eccentricity is high then the UMP will be excessive generating high audible noise (which will flag up a developing fault when inspected) or complete rotor pull-over in the air-gap which will cause drive failure. These machines are often servo drives and under AC (sine wave current) control. However, brushless DC (trapezoidal current) control will also be investigated.

II. ANALYTICAL ANALYSIS

In this section an analytical model is put forward to help identify the sources of UMP and quantify the frequency of any vibrations. Fractional-slot brushless permanent magnet motors have a complex spectrum of flux waves in the air-gap. In this section we will briefly investigate the flux wave terms and calculation of UMP.

A. Rotating Air-gap Flux waves and Unbalanced Magnetic Pull

UMP is generally calculated using the approximation for the normal stress around a closed contour in the air-gap. If F_x is the force in the x direction then

$$F_x = L\int_0^{2\pi r} \frac{b_n(y,t)^2}{2\mu_0}\cos\left(\frac{y}{r}\right)dy \tag{1}$$

where r is the radius of the contour and y is the linearised distance around the contour. It is commonly known that UMP will be generated when there are two air-gap flux waves with pole-pair numbers differing by one [9]. The relative rotational velocities of the waves will dictate as to whether the force is a steady pull or a pulsating force. Multiplying to flux waves together with pole pair differing by one gives

$$\begin{aligned} b_n(y,t)^2 &= \mathrm{Re}\left[\overline{B}_n e^{j(\omega_n t - nky)}\right]\times\mathrm{Re}\left[\overline{B}_m e^{j(\omega_m t - mky)}\right] \\ &= \frac{1}{2}\mathrm{Re}\left[\overline{B}_n\overline{B}_m e^{j(\omega_n t - nky)}e^{j(\omega_m t - mky)} + \overline{B}_n\overline{B}_m^* e^{j(\omega_n t - nky)}e^{-j(\omega_m t - mky)}\right] \\ &= \frac{1}{2}\mathrm{Re}\left[\overline{B}_n\overline{B}_m e^{j((\omega_n+\omega_m)t-(n+m)ky)} + \overline{B}_n\overline{B}_m^* e^{j((\omega_n-\omega_m)t-(n-m)ky)}\right] \end{aligned} \tag{2}$$

We can find the forces in two perpendicular radial directions. The force on the x axis is

$$\begin{aligned} F_x &= L\int_0^{2\pi r}\frac{b^{/}(y,t)^2}{4\mu_0}(e^{jky}+e^{-jky})\,dy \\ &= \frac{L}{8\mu_0}\int_0^{2\pi r}\mathrm{Re}\left[\begin{array}{l}\overline{B}_n\overline{B}_m e^{j((\omega_n+\omega_m)t-(n+m)ky)} \\ +\overline{B}_n\overline{B}_m^* e^{j((\omega_n-\omega_m)t-(n-m)ky)}\end{array}\right](e^{jky}+e^{-jky})\,dy \end{aligned} \tag{3}$$

This then becomes

$$F_x = \frac{\pi r L}{4\mu_0}\mathrm{Re}\left[\begin{array}{l}\overline{B}_n\overline{B}_m e^{j(\omega_n+\omega_m)t}\Big|_{n+m=1} + \overline{B}_n\overline{B}_m e^{j(\omega_n+\omega_m)t}\Big|_{n+m=-1} \\ +\overline{B}_n\overline{B}_m^* e^{j(\omega_n-\omega_m)t}\Big|_{n-m=1} + \overline{B}_n\overline{B}_m^* e^{j(\omega_n-\omega_m)t}\Big|_{-n+m=1}\end{array}\right] \quad (4)$$

And for the force on the *y* (vertical) axis

$$\begin{aligned} F_y &= L\int_0^{2\pi r}\frac{b^{/}(y,t)^2}{4\mu_0 j}(e^{jky}-e^{-jky})\,dy \\ &= \frac{L}{8\mu_0}\int_0^{2\pi r}\mathrm{Im}\left[\begin{array}{l}\overline{B}_n\overline{B}_m e^{j((\omega_n+\omega_m)t-(n+m)ky)} \\ +\overline{B}_n\overline{B}_m^* e^{j((\omega_n-\omega_m)t-(n-m)ky)}\end{array}\right](e^{jky}-e^{-jky})\,dy \end{aligned} \quad (5)$$

$$F_y = \frac{\pi r L}{4\mu_0}\mathrm{Im}\left[\begin{array}{l}\overline{B}_n\overline{B}_m e^{j(\omega_n+\omega_m)t}\Big|_{n+m=1} + \overline{B}_n\overline{B}_m e^{j(\omega_n+\omega_m)t}\Big|_{n+m=-1} \\ -\overline{B}_n\overline{B}_m^* e^{j(\omega_n-\omega_m)t}\Big|_{n-m=1} - \overline{B}_n\overline{B}_m^* e^{j(\omega_n-\omega_m)t}\Big|_{-n+m=1}\end{array}\right] \quad (6)$$

This illustrates that UMP is generated by pole-pair numbers varying by one. We can use the expressions for the UMP to identify the pole number combinations that result in UMP.

B. Rotor air-gap flux waves

The magnets will produce a trapezoidal shaped rotating flux and this can be put into a complex form [9] where

$$b_r(\theta,t) = \sum_m B_r^m \cos mp(\omega_r t-\theta+\phi_m) = \mathrm{Re}\sum_m \frac{\overline{B}_r^m}{2}e^{jmp(\omega_r t-\theta)} \quad (7)$$

where m = 1, 3, 5, etc. If we include the stator slotting n_s and restrict the harmonic number to the stator slot number then

$$\begin{aligned} b_r(\theta,t) &= \sum_m B_r^m\left[\cos mp(\omega_r t-\theta+\phi_m)\left(1+\lambda_{slot}\cos n_s\theta\right)\right] \\ &= \mathrm{Re}\sum_m \frac{\overline{B}_r^m}{2}\left[\left(e^{jmp(\omega_r t-\theta)}\right)\left(1+\frac{\lambda_{slot}}{2}\left(e^{jn_s\theta}+e^{-jn_s\theta}\right)\right)\right] \end{aligned} \quad (8)$$

C. Stator air-gap flux waves

Let us assume that the winding is a balanced 3-phase winding. However, in a fractional slot machine it should not be assumed that the winding MMF is made with a fundamental pole-pair harmonic with 5th, 7th, 11th,13th, etc windings. We have to take the fundamental harmonic as two for the general case and eliminate harmonics if they are zero. Hence

$$\begin{aligned} b_s(\theta,t) &= \sum_{n_w} B_s^{n_w}\cos(\omega_s t-n_w\theta+\phi_m) \\ &= \mathrm{Re}\sum_{n_w}\frac{\overline{B}_s^{n_w}}{2}e^{j(\omega_s t-n_w\theta)} = \mathrm{Re}\sum_{n_w}\frac{\overline{B}_s^{n_w}}{2}e^{j(p\omega_r t-n_w\theta)} \end{aligned} \quad (9)$$

where n_w is the winding harmonic of the non symmetrical windings (shown below) Equations (8) and (9) can be used and put into (4) and (6) to identify UMP components and frequencies.

D. Rotor Eccentricity

Rotor eccentricity can be denoted using the method as described in [8] using permeance modulation so that the magnet flux wave can be represented as

$$\begin{aligned} b_r(\theta,t) &= \mathrm{Re}\sum_m \frac{\overline{B}_r^m}{2}e^{jm(\omega_r t-p\theta)}\left(\begin{array}{l}1+\frac{\lambda_{slot}}{2}\left(e^{jn_s\theta}+e^{-jn_s\theta}\right) \\ +\frac{\lambda_{ecc}}{2}\left(e^{j\theta}+e^{-j\theta}\right)\end{array}\right) \\ &= \mathrm{Re}\sum_m\left(\begin{array}{l}\frac{\overline{B}_r^m}{2}e^{jm(\omega_r t-p\theta)}+\frac{\lambda_{slot}\overline{B}_r^m}{4}e^{j(m\omega_r t-(mp\pm n_s)\theta)} \\ +\frac{\lambda_{ecc}\overline{B}_r^m}{4}e^{j(m\omega_r t-(mp\pm 1)\theta)}\end{array}\right) \end{aligned} \quad (10)$$

where n_s is the slot number. This equation is for static eccentricity and includes slotting. It can be seen that eccentricity modulates that MMF to produce air-gap flux waves that vary by one pole-pair, i.e., the criterion for UMP is met. This assumes that the eccentricity is restricted to the first permeance harmonic (in a similar way to the slot permeance modulation approximation).

Static eccentricity is where the rotor is rotates on its own axis but is not centered on the stator bore axis. This could be caused by out of tolerance, misplaced or worn mountings or bearings. Dynamic eccentricity is where the rotor does not rotate on its own axis but does rotate on the stator axis so that the point of minimum air-gap rotates with rotor speed. This could be caused by a bent shaft or out of tolerance manufacturing.

A similar equation exists for the stator air-gap fluxes:

$$\begin{aligned} b_s(\theta,t) &= \mathrm{Re}\sum_m \frac{\overline{B}_s^n}{2}e^{j(\omega_r t-np\theta)}\left(\begin{array}{l}1+\frac{\lambda_{slot}}{2}\left(e^{jn_s\theta}+e^{-jn_s\theta}\right) \\ +\frac{\lambda_{ecc}}{2}\left(e^{j\theta}+e^{-j\theta}\right)\end{array}\right) \\ &= \mathrm{Re}\sum_m\left(\begin{array}{l}\frac{\overline{B}_s^n}{2}e^{j(\omega_r t-np\theta)}+\frac{\lambda_{slot}\overline{B}_s^n}{4}e^{j(\omega_r t-(np\pm n_s)\theta)} \\ +\frac{\lambda_{ecc}\overline{B}_s^n}{4}e^{j(\omega_r t-(np\pm 1)\theta)}\end{array}\right) \end{aligned} \quad (11)$$

where for a balanced 3-phase machine n = 1, -5, 7, etc, in the usual sequence. Note that the time component is now $\omega_r t$ in (11) rather that $m\omega_r t$ in (10). This will lead to different vibration components when the machine is open-circuit (when there are only rotor flux wave components) and loaded (when there are both stator and rotor flux wave components).

III. Machine Examples

Several machine examples are put forward in the paper. The focus will be on two 9 slot machines – one with 8 poles and one with 6 poles (surface magnets) and three 18 slot machines – two with 12 poles (one with surface magnets and one with a consequent-magnet rotor) and one with 16 surface-magnet poles. All the machines have surface ferrite magnet rotors. Ferrite was purposely chosen for this study in order to eliminate potential unknowns related to losses in the magnets and to provide a relatively low magnetic loading that would limit saturation and enable a more straightforward comparison of numerical and analytical results. Internal PM rotors with NdFeB magnets will be the focus of future work. The machines

are modeled in *SPEED* PC-BDC [11] to examine the winding layout harmonics then passed through to the finite element package PC-FEA [12] to obtain the UMP under different loading conditions. The teeth are bifurcated. The machines have the same air-gap length, axial length, electric loading and diameter and the nominal specifications are given in Table I. The machines will be simulated at a speed on 500 rpm and the full-load torques are given at 4.5 A (on the q-axis). The amp-turns and the basic geometry (including the axial length) are identical for all machines. This allows direct comparison.

TABLE I. MACHINE PARAMETERS AND RATINGS

Parameter		Value
Stator OD		136.5 mm
Rotor OD		77.6 mm
Full-load current		4.5 A
Magnet B_r		0.38 T
Full Load Torque obtained from PC-BDC [slot number/pole number]	9/8	3.75 Nm
	9/6	3.15 Nm
	18/12 double layer	3.27 Nm
	18/16 double layer	3.85 Nm
	8/12 consequent	2.40 Nm

A. 9 slot machines

In Fig. 1 the 9 slot machines are shown. The top machine (8 pole) shows the that winding a non symmetrical compared to the 6 pole machine and this is reflected in the winding harmonic distribution as shown, where the 8 pole machine has many harmonics, including sub harmonics (below 4). The 8 pole machine was shown to exhibit high UMP under loading in [7] and it is obvious from the winding layout that there will be a pull towards the excited winding due to asymmetry. The 6 pole machine has a symmetrical winding however the rotor pole – stator slot combination is asymmetrical. This can be identified by the fact that rotor pole faces are diametrically opposite each other whereas a tooth and a slot opening are diametrically opposite. This will produce UMP due to asymmetry.

We can go through an exercise to identify the UMP components for the 9 slot 8 pole machine since this will produce UMP even without rotor eccentricity. In Table II the air-gap flux waves are tabulated to identify the pole numbers and associated vibration frequencies. Table III gives an example of matching pole-pair numbers and the resulting vibration components. In [7] it was shown that the asymmetrical winding dominates the UMP and this has a vibration of $8\omega_r$ which is twice the supply frequency. Similar tables can be developed for all the machines when eccentricity is included in the table.

TABLE II. ROTOR AND STATOR AIR-GAP FLUX WAVES FOR 9 SLOT 8 POLE MACHINE

	Rotor Flux Waves					
m	1	3	5	7	9	11
pm	4	12	20	28	36	44
pm-n_s	-5	3	11	19	27	35
pm+n_s	13	21	29	37	45	53
ω_r coefficient	4	12	20	28	36	44
	Stator Flux Waves					
n_w	1	-2	4	-5	7	-8
ω_r coefficient	4	4	4	4	4	4

TABLE III. VIBRATION COMPONENTS FOR MATCHING POLE-PAIR NUMBERS (NOT A COMPLETE LIST)

Rotor-rotor	4 and -5	4 and 3	12 and 13
ω_r coefficient vibration	8	8	8
Stator-stator	1 and -2	4 and -5	7 and -8
ω_r coefficient vibration	8	8	8
stator-rotor	4 and -5	-5 and 4	-11 and 12
ω_r coefficient vibration	8	8	16

In (10) and (11) it is seen that the slotting of the stator will also interact with the magnets to possibly generate additional waves which may produce some UMP.

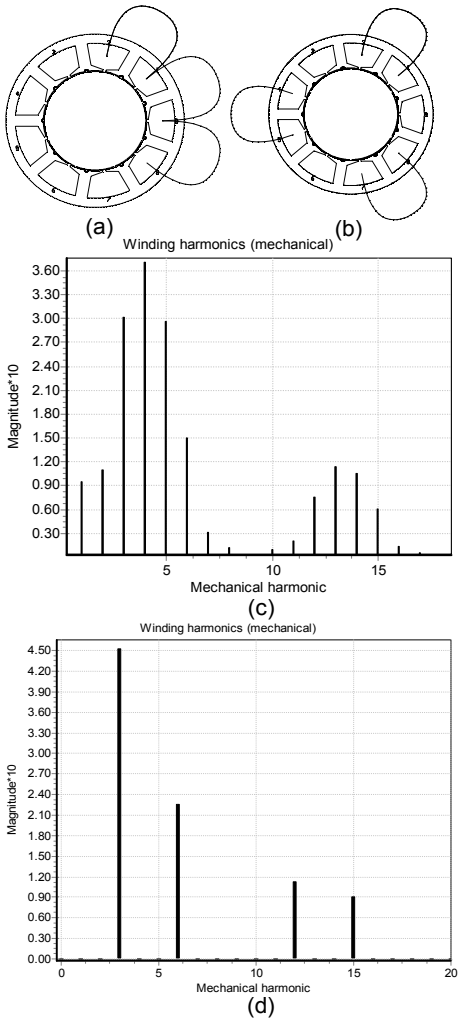

Fig. 1. 9 slot 8 pole machine - (a) and (c), and 9 slot 6 pole machine - (b) and (d); showing one phase of the 3-phase winding and phase winding harmonic.

B. 18 slot machines

Figs. 2 and 3 show the 18 slot machines with single and double layers while Figs. 4 and 5 repeat this for the 12 pole arrangement. While none of these machines have an asymmetrical windings (as with the 9 slot 8 pole machine) the 16 pole machine has a series of winding harmonics starting from a 4 pole (double layer) or 2 pole (single layer) harmonic that may produce higher UMP when there is some eccentricity. This is examined in the FEA analysis.

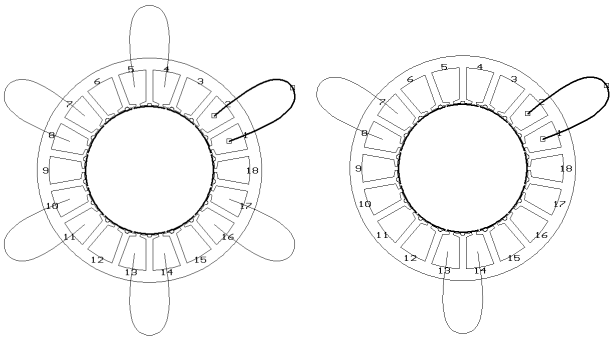

(a) (b)

Fig. 2. Phase winding distribution for 18 slots 12 pole – (a) double-layer configuration and (b) single-layer configuration

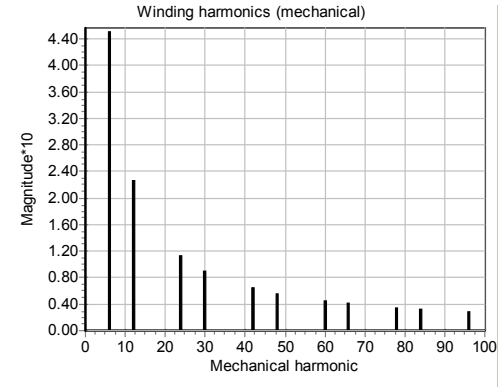

(a)

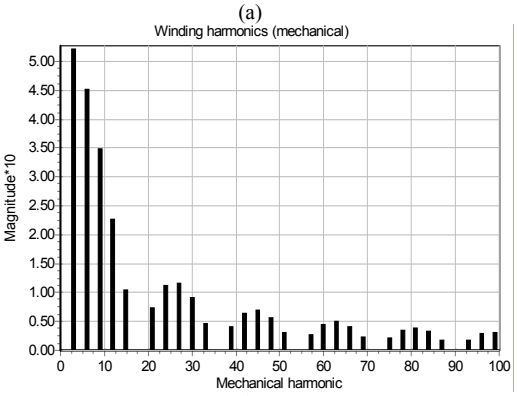

(b)

Fig. 3. Mechanical MMF harmonics for 18 slots 12 pole configuration – (a) double-layer configuration and (b) single-layer configuration.

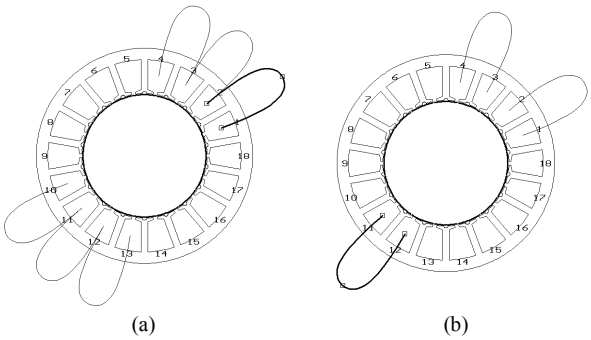

(a) (b)

Fig. 4. Phase winding distribution for 18 slots 16 pole machine – (a) double-layer configuration and (b) single-layer configuration

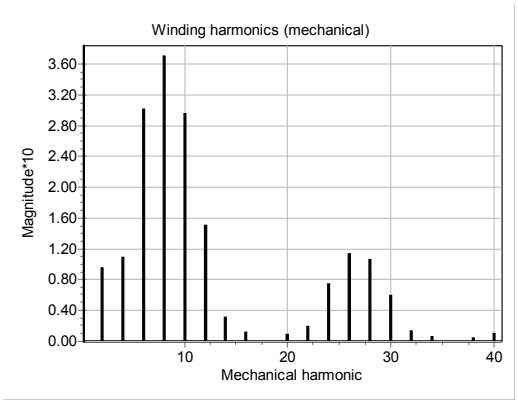

(a)

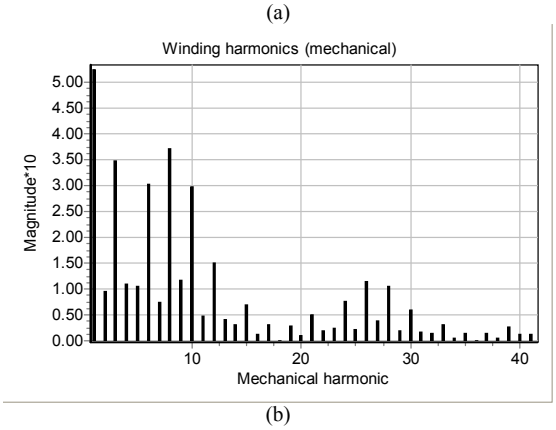

(b)

Fig. 5. Mechanical MMF harmonics for 18 slots 16 pole machine – (a) double-layer configuration and (b) single-layer configuration.

IV. FINITE ELEMENT MODELING

A. Centered rotor UMP in 9 slot 8 pole machine

The flux wave harmonics are complex in a fractional slot machine so that to obtain accurate values for the UMP then finite element analysis is used to calculate it. Once a solution is obtained then a closed contour of the radial air-gap flux density can be obtained and the UMP calculated by implementing (3) and (5) in an elemental form. The UMP for the 9 slot 8 pole machine when the rotor is centered and open circuit and fully loaded are put forward in Fig. 6. On the left are flux plots while the the UMP results when fully loaded and open-circuit are shown on the right. It can be seen that the UMP oscillates twice with 90 mechanical degrees of movement which represents one cycle of the current (which here is sinusoidal). This is predicted in Table III under the stator-stator column. On the right is the UMP on open circuit. There are $8\omega_r$ vibrations as predicted in Table III. In addition, there is a steady pull and a twice supply frequency vibration which would be identified with further extension of the table. It can be seen that the open-circuit UMP is much less than the full load UMP due to the asymmetry. The magnets are ferrite magnets and the slot openings are narrow. The UMP under full load suggests that the machine is liable to experience high bearing wear during full-load operation. There does look to be some asymmetry in the flux plot in Fig. 6(c) on open-circuit

however the imbalance of flux in the air-gap is much less due to ripple flux across the stator teeth tops. This can be observed by the even flux in the magnets.

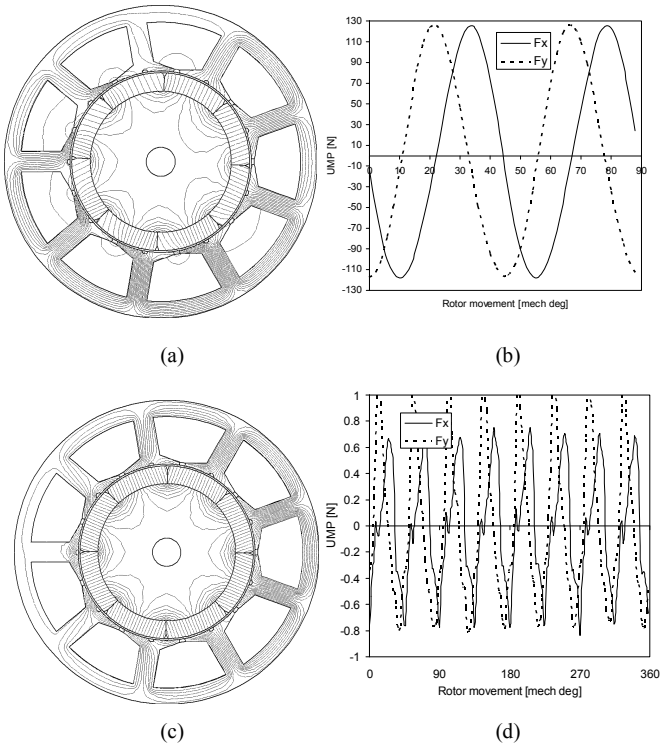

Fig. 6. 9 slot 8 pole machine (a) flux plot when fully loaded, (b) UMP in *x* and *y* directions over 90 mech deg rotor movement at full loading, (c) flux density distribution under open-circuit operation and (d) UMP in *x* and *y* directions under open-circuit conditions over 360 mech deg.

B. Centered rotor UMP in 9 slot 6 pole machine

This machine is likely to have much less UMP than the 8 pole machine due to the fact that the stator winding is symmetrical. The open circuit UMP is shown in Fig. 7. It can be seen that there is very little UMP in the *x* (horizontal) direction and negligible in the *y* direction. When loaded, the balanced winding leads to similar negligible results so they are omitted here. The frequency of the low-level vibration can be observed to be equal to the pole number.

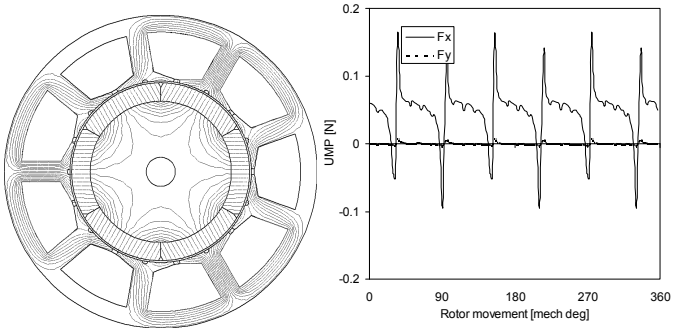

Fig. 7. 9 slot 6 pole machine flux density distribution under open-circuit operation and UMP in *x* and *y* directions.

C. 10 % eccentricity in 18 slot 16 pole surface-magnet machines

The 9 slot 8 pole machine has inherent asymmetry. The other machines do not have this asymmetry when the rotor is centered in the stator bore. However, there is always some degree of eccentricity due to tolerance variation and also wear and here it is examined using the variation of static eccentricity. The rotor is displaced in the *x* direction and the simulation carried out. We will investigate 10 % static eccentricity in the 18 slot machines to highlight the effect. Fig. 8 gives the UMP under these conditions under open-circuit (d) and full load conditions (b), for the double layer winding. The UMP during open circuit operation is almost constant when fully-loaded there is a vibration component. The rotation is 45 mechanical degrees which is movement of 2 rotor poles or one cycle of the current. The UMP has a constant pull of 25 to 30 N and a 10 N peak-to-peak oscillation. The oscillation is $2 \times 8 = 16$ times the rotational frequency which is again equal to the pole number (as with the 9/8 and 9/6 machines).

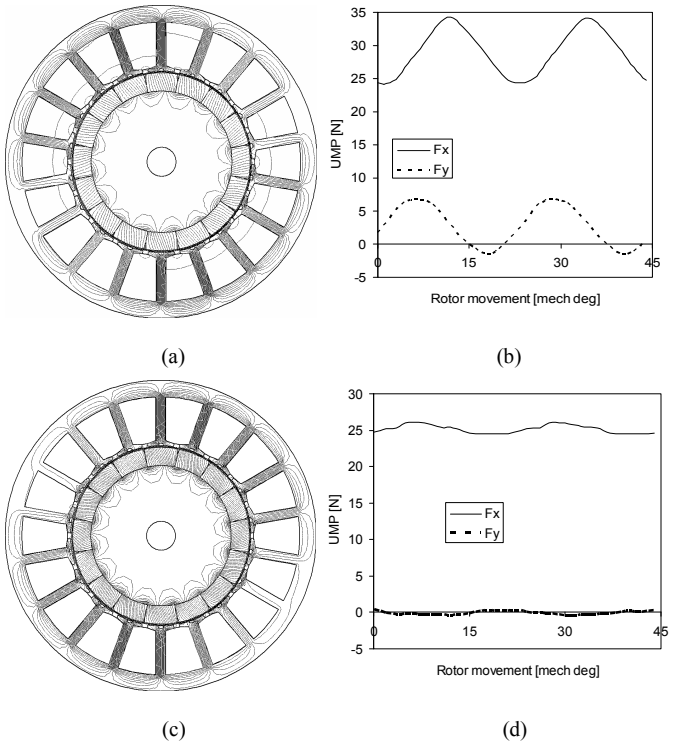

Fig. 8. 18 slot 16 pole machine with double-layer winding and 10 % eccentricity (a) flux plot when fully loaded, (b) UMP in *x* and *y* directions over 45 mech deg rotor movement at full loading, (c) flux density distribution under open-circuit operation and (d) UMP in *x* and *y* directions under open-circuit conditions over 45 mech deg.

Since there is 10 % static rotor eccentricity then even with a symmetrical rotor/stator arrangement there is still UMP and this can be seen in Fig. 8(d). There is a steady pull in the direction on minimum air-gap length as would be expected since there will be high flux density around this point.

In Fig. 9 the 18/16 machine is investigated with the single layer winding in Fig 4(b). It can be seen that there is now a much higher vibration component in the UMP when using the

single layer winding due to the high winding harmonic component – particularly in the single-layer winding where there is a 2-pole sub-harmonic (Fig.5(b)).

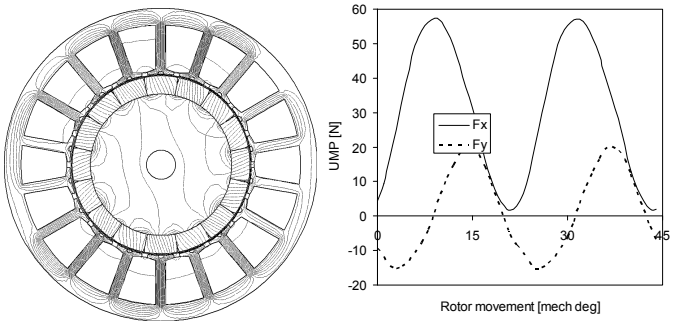

Fig. 9. 18 slot 16 pole machine with single-layer winding and 10 % eccentricity, flux plot when fully loaded and UMP in *x* and *y* directions over 45 mech deg rotor movement at full loading.

D. 10 % eccentricity in 18 slot 12 pole machine

The 18 slot 12 pole UMP results are shown in Fig. 10. These are for open-circuit and loaded conditions (double and single layer). It can be seen that the UMP for the 12 pole machine is just under 25 N – this is a steady pull . This rotor movement is over 60 mechanical degrees and it shows a minor 36-times rotational frequency vibration. The UMP appears to be dominated by the rotor magnetic forces interacting with the eccentricity. The winding harmonics are more sparse for the 12 pole machine (Fig. 3) and the lower sub-harmonic is 3 (6-pole).

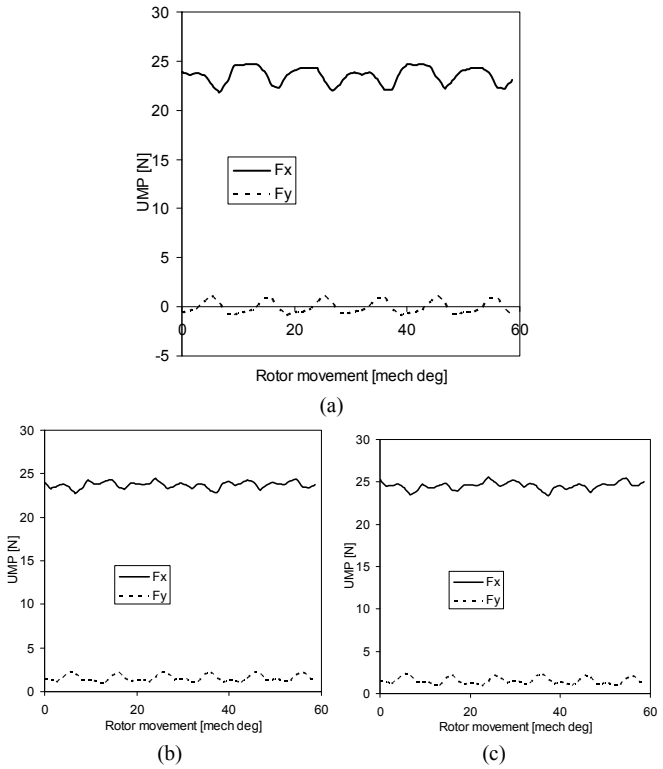

Fig. 10. UMP in 18 slot 12 pole machine with 10 % eccentricity over 60 mech. deg.; (a) open-circuit, (b) loaded double-layer winding and (c) loaded single layer winding.

E. 10 % eccentricity in 18 slot 12 consequent pole machine

It was mentioned earlier that other machine arrangements will be investigated. A simple comparison here can be made to a consequent pole machine, where every second pole is steel so that the number of magnets is equal to the number of pole pairs. In Table I it can be seen that this machine actually produces less torque since the amount of magnet material is halved. Often, thicker magnets are used in a consequent-pole machine but here we will maintain them at a constant thickness and strength.

For direct comparison, alternate magnets in the 18 slot 12 pole machine (with double and single layer winding) were changed to steel in the FEA model. The UMP for these arrangements are shown in Fig. 11. It can be seen that the UMP is now much higher, up to four times, for the consequent pole machine and the peak is about 100 N. This is because steel rotor poles considerably reduce the air-gap length and modifies the air-gap permeance so that there is a much high imbalance in air-gap flux due to the 10 % eccentricity. This also has an advantage when applied to a bearingless machine [10].

A flux plot for the consequent pole machine is shown in Fig. 12 when loaded using the single-layer winding. It is still difficult to observe the flux imbalance even at these higher UMP values. This also shows the consequent arrangement of the magnets in the rotor.

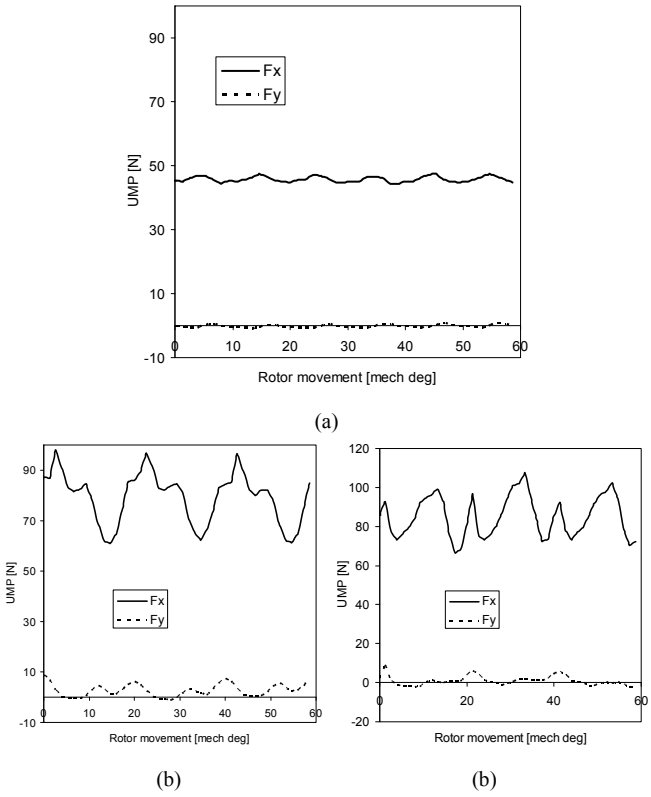

Fig. 11. UMP in 18 slot 12 consequent pole machine with 10 % eccentricity over 60 mech. deg.; (a) under open-circuit and loaded with double-layer winding (b) and single-layer winding (c).

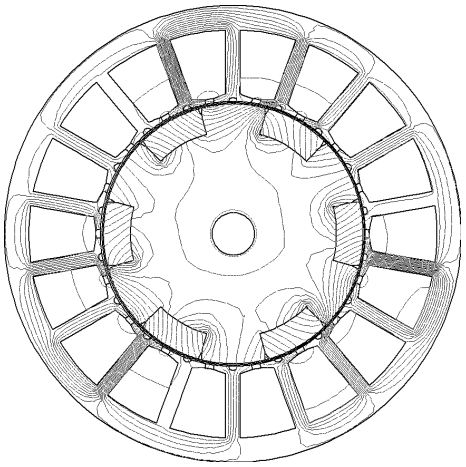

Fig. 12. Flux plot in 18 slot 12 consequent pole machine with 10 % eccentricity and loaded with single-layer winding.

F. 10 % eccentricity in 18 slot 16 consequent pole machine

It can be seen in sections IV.*D* and IV.*E* that moving from surface-magnet to consequent-poles in the 18/12 machine increased the UMP and also increased the UMP due to loading (loading had a minimal effect in the surface-magnet arrangement). Therefore is it is worthwhile investigating the UMP in a consequent-pole 18/16 machine on open-circuit and when loaded using the single-layer winding. Fig. 13 gives the UMP under these situations. On open-circuit the UMP is almost doubled compared to the surface magnet arrangement however under the loading the UMP. When the machine is loaded using the single-layer winding the UMP increases many fold. The *x*-axis (direction of eccentricity) UMP has an 8 times rotational frequency with a peak-to-peak force of over 400 N and a steady pull of about 150 N. There is also a peak-to-peak vibration of 400 N in the perpendicular direction. This machine is likely to generate much noise with low amounts of rotor eccentricity. A flux plot is shown in Fig. 14 for the loaded condition at the zero degree location. This time it is possible to see and imbalance in flux and at this point there is a 200 N force in the vertical direction.

Therefore it can be concluded that under some circumstances consequent-pole machines can generate high UMP with even low-level eccentricity when the windings have a high harmonic content.

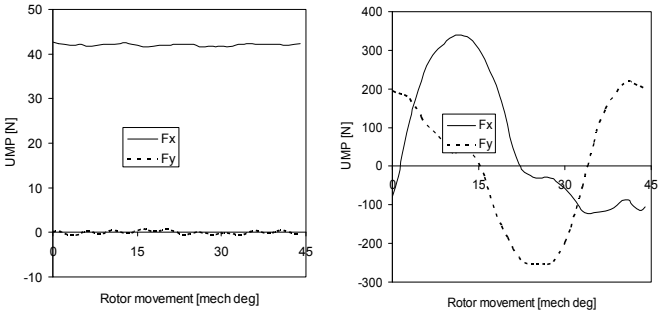

Fig. 13. UMP in 18 slot 16 consequent pole machine with 10 % eccentricity over 45 mech deg.; (a) under open-circuit and (b) loaded single-layer winding.

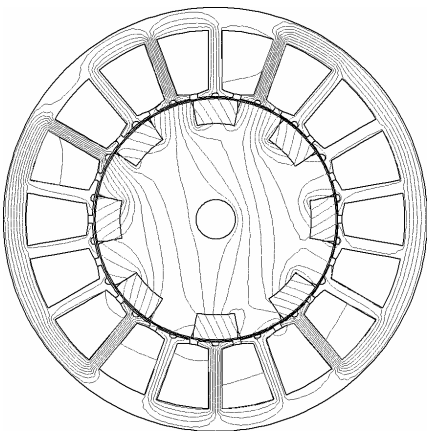

Fig. 14. Flux plot in 18 slot 16 consequent pole machine with 10 % eccentricity and loaded with single-layer winding.

G. DC operation in 18 slot 12 pole machine with 10 % eccentricity

These machines examples used in this paper are suitable for brushless AC (sinewave current) control. However analysis of the back-EMF waveform for the 18 slot 12 pole machine with a double-layer winding suggests it may also be possible to control this machine effectively using DC control. The back-EMF waveform is shown in Fig. 15.

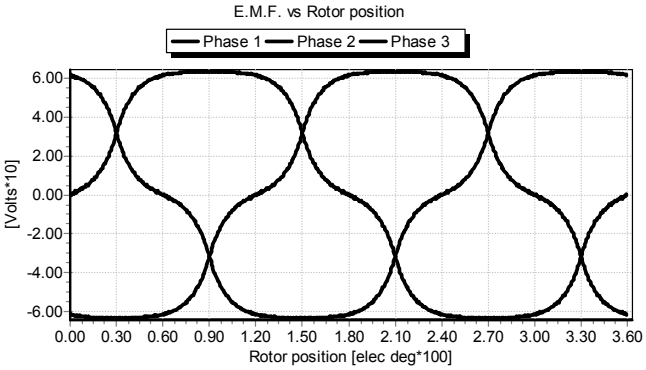

Fig. 15. Back-EMF waveform for 18/12 machine with double layer winding (taken from PC-BDC).

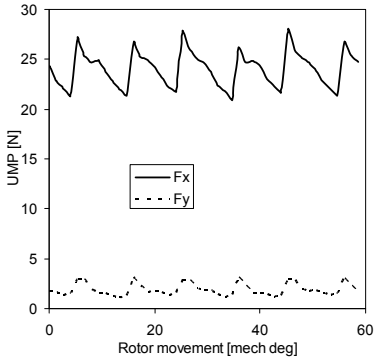

Fig. 16. UMP in 18 slot 12 pole machine under DC control with 10 % eccentricity over 60 mech. deg and double-layer winding.

If brushless DC control is used then the UMP is shown in Fig. 16. This can be compared to Fig. 9(b). It can be seen that the brushless DC control produces UMP vibration. This is a saw-tooth waveform therefore it will consist of a harmonic series of vibration frequencies.

H. Effect of 10 % eccentricity on the torque of an 18 slot 16 pole machine with single layer winding

Space constrains prevent a full analysis of the effect of eccentricity on the torque however it can be seen in Fig. 9 that the 18/16 machine with double layer produces UMP vibration. Therefore here the change in torque will also be investigated using the current – flux linkage (I-Psi) loops. This is an effective way to calculate the mean torque and the argument will be restricted to this. In Fig. 17 the I-Psi loops are shown when the rotor is eccentric and also when centered. From PC-FEA (rather than PC-BDC as given in Table I) the centered-rotor torque is 4.3 Nm and the 10 % eccentric value is 3.9 Nm. This is a 10 % decrease in torque – this needs further investigation through experiment. The loops for phase 1 are given in Fig. 17 and the other phases loops do follow the same respective orbits.

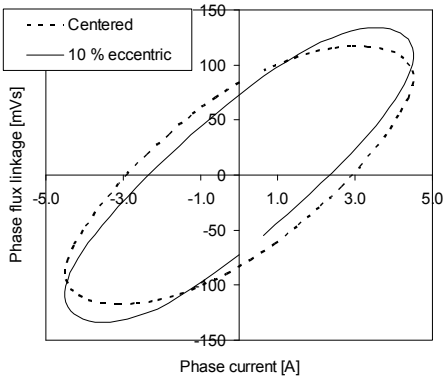

Fig. 17. I-Psi loops for phase 1 when rotor is centered and 10 % eccentric (from PC-FEA).

V. CONCLUSIONS

This paper has addressed the issue of UMP in fractional slot brushless permanent magnet machines. An analytical algorithm is first developed which illustrates how it is possible to identify the different components in the UMP. After this a more detailed approach is taken via the use of finite element analysis and this was used under many different machine arrangements.

The work here is couched in terms of AC operations with some DC control briefly addressed (which produced more UMP vibration due to switching effects). The work illustrates that some machine arrangements will be very susceptible to UMP when eccentricity is present and also they may be a source of noise and vibration. Different winding configurations are inspected and these can produce larger values of UMP. Consequent-pole rotors are also addressed and these generally produce higher UMP compared to their surface-magnet counterpart. Some of the results indicate that for certain motor designs eccentricity can cause, apart from UMP, a reduction in the average output torque.

ACKNOWLEDGEMENT

The authors are grateful for the kind co-operation of AO Smith Corp. in the preparation of this paper.

REFERENCES

[1] A. Burakov and A. Arkkio, “Comparison of the Unbalanced Magnetic Pull Mitigation by the Parallel Paths in the Stator and Rotor Windings”, IEEE Trans on Magnetics, Volume 43, No. 12, Dec. 2007, pp 4083 – 4088.

[2] D. G. Dorrell, “Experimental behaviour of unbalanced magnetic pull in 3-phase induction motors with eccentric rotors and the relationship with tooth saturation”, IEEE Trans on Energy Conversion, Volume 14, Issue 3, Sept. 1999, pp 304 – 309.

[3] R. Perers, U. Lundin and M. Leijon, “Saturation Effects on Unbalanced Magnetic Pull in a Hydroelectric Generator With an Eccentric Rotor”, IEEE Trans on Magnetics, Vol. 43, No. 10, Oct 2007, pp 3884-3890.

[4] C. BI, N. L. H. Aung, H. N. Phyu, Q. Jiang, and S. Lin, “Unbalanced Magnetic Pull Induced by Drive Current In PM-BLDC Motor Operation”, International Conference on Electrical Machines and Systems 2007, Oct. 8~11, Seoul, Korea.

[5] C. Bi, Z.J. Liu, T.S. Low, “Effects of Unbalanced magnetic Pull in Spindle Motors”, IEEE Trans Mag, Vol. 33, No. 5, Sept 1997.

[6] D. G. Dorrell, "The sources and characteristics of unbalanced magnetic pull in cage induction motors with either static or dynamic eccentricity", Stockholm Power Tech, IEEE International Symposium on Electric Power Engineering, Stockholm, Sweden, 18-22 June 1995, Volume on Electrical Machines and Drives pp 229-234.

[7] P. Vijayraghavan and R. Krishnan, “Noise in electric machines: a review”, IEEE Trans on Industry Applications, Vol. 35, No. 5, Sep/Oct 1999, pp 1007 – 1013.

[8] Z. Q. Zhu, D. Ishak, D. Howe, and J. Chen, “Unbalanced Magnetic Forces in Permanent-Magnet Brushless Machines With Diametrically Asymmetric Phase Windings”, IEEE Trans on Industry Applications, Vol. 43, No. 6, Nov/Dec 2007.

[9] A. C. Smith and D. G. Dorrell, "The calculation and measurement of unbalanced magnetic pull in cage induction motors with eccentric rotors. Part 1: Analytical model", 1996 Proc. IEE Electric Power Applications, Vol. 143, No. 3, pp 193-201.

[10] D. G. Dorrell, J. Amemiya, A. Chiba and T. Takenaga, ”Analytical modelling of a Consequent-Pole Bearingless Permanent Magnet Motor”, IEEE International Conference on Power Electronics and Drive Systems, Singapore, 17 -19 Nov, 2003.

[11] TJE. Miller and M. I. McGilp, “PC-BDC 8.0 for Windows – Software”, SPEED Laboratory, University of Glasgow, Glasgow (UK), 2008.

[12] M.Olaru, TJE Miller and M. I. McGilp, “PC-FEA 5.5 for Windows – Software”, SPEED Laboratory, University of Glasgow, Glasgow (UK), 2007.